CLTRN, regulated by NRF1/RAN/DLD protein complex, enhances radiation sensitivity of hepatocellular carcinoma cells through ferroptosis pathway

Yin Yuan
First Affiliated Hospital of Soochow University
Wen Cao
Affiliated Hospital of Nantong University
Hongbing Zhou
Affiliated Hospital of Nantong University
Haixin Qian (3410634395@qq.com)
Honggang Wang
Affiliated Hospital of Nantong University

Research

Keywords: HCC, CLTRN, radiation sensitivity, ferroptosis

Posted Date: July 6th, 2020

DOI: https://doi.org/10.21203/rs.3.rs-39620/v1

Version of Record: A version of this preprint was published at International Journal of Radiation Oncology*Biology*Physics on July 1st, 2021. See the published version at https://doi.org/10.1016/j.ijrobp.2020.12.062.

Abstract

Background

Radiotherapy is a viable treatment option for patients with unresectable hepatocellular carcinoma (HCC). However, radiation resistance is an issue that needs to be addressed. In this context, cumulative evidence supports the functional roles of a variety of RNA or proteins in radioresistance, and suggests that the modulation of their expression may constitute a novel radiosensitization approach. Here, we investigated the ability of collectrin (CLTRN) to enhance the radiosensitivity in HCC patients for the first time.

Methods

Transcriptome sequencing technology (RNA-seq technology) was used to analyze the transcription-level changes in the genes from the HepG2 cells before and after X-ray irradiation. Combining the results with the HCC tissue RNA-seq data, we determined the ultimate target gene through bioinformatics analysis and cellular verification. A series of cellular and molecular biology techniques were applied in vitro and in vivo to confirm whether CLTRN can enhance radiosensitivity in HCC cells. Subsequently, the downstream action mechanism, the upstream transcription factor, and the interaction proteins of CLTRN were determined.

Results

First, we confirmed the association between CLTRN and radiosensitivity. We observed that CLTRN overexpression led to a significant reduction in the proliferation, migration, and invasion potential of X-ray-irradiated HCC cells, whereas no observable effect was exerted on cell cycle and apoptosis. The same results were observed in nude mice in vivo. Investigation of the gene regulatory mechanism revealed that the genes analyzed at transcriptome level after CLTRN overexpression were mostly enriched in the glutathione metabolic pathway. As glutathione metabolism forms a vital link in ferroptosis, we surmised that CLTRN is associated with ferroptosis. This was confirmed through the detection of cellular iron, ROS level determination, transmission electron microscopy, and monitoring of ferroptosis-related protein indicators. Lastly, we investigated whether nuclear respiratory factor 1 (NRF1) is the upstream transcription factor of CLTRN, and whether dihydrolipoamide dehydrogenase (DLD) and members of the RAS oncogene family (RAN) are its interacting proteins.

Conclusion

Our results indicate that CLTRN is a vital regulator of radiation sensitivity and could serve as a novel therapeutic target or prognostic marker in HCC treatment.

Background

Hepatocellular carcinoma (HCC) is the most common cancer among adults and causes approximately 740,000 deaths worldwide[1]. HCC is highly prevalent in China, where new cases and deaths from HCC account for more than half of its global sum[2]. Clinically, only approximately 30% of HCC patients are eligible for operative treatment, although the prognosis remains poor[3]. In addition, non-surgical treatment is particularly important for patients with unresectable HCC or elderly patients who are not eligible for surgery. At present, the most important non-surgical treatments for tumor patients include radiotherapy, chemotherapy, and molecular targeted therapy among others. Although radiotherapy is one of the most important non-surgical methods for tumor treatment, it has limited applicability in HCC owing to the low radiation tolerance of normal liver cells and the inherent radiation resistance in HCC[4]. Therefore, improving the sensitivity of HCC cells to chemotherapy has posed a challenge in the study of liver cancer.

An increasing number of genes, including those for non-protein-coding and protein-coding RNA, are considered to be associated with radiosensitivity of tumors. In prostate cancer, poly (ADP-ribose) polymerase 1(PARP-1) is thought to increase the sensitivity of tumor cells to radiation therapy[5]. In addition, miR-205 enhances radiosensitivity of prostate cancer cells by impairing DNA damage repair through the inhibition of protein kinase C, epsilon (PKCε), and zinc finger E-box binding homeobox 1(ZEB1)[6]. In HCC, miR-621 acts as a tumor radiosensitizer by directly targeting SETDB1[7]. In colorectal cancer cells, the downregulation of long noncoding RNA UCA1 enhances radiosensitivity and inhibits migration of tumor cells by suppressing epithelial-mesenchymal transition[8].

Here, we screened a radiation-sensitive gene, CLTRN, using RNA-seq technology, and studied the upstream and downstream mechanisms of action in HCC.

Patients And Methods

Patients and tissue samples

A total of 109 patients were enrolled in the present study. Patients underwent curative resection for HCC at the Department of Hepatobiliary Surgery of the Fifth Affiliated Hospital of Medical School of Nantong University (Taizhou, China) between January 2012 and December 2014. Patients did not receive any treatments before surgery. They were followed up after surgery until January 2019, with a median follow-up of 30 months (range, 4-70 months). During the follow-up, patients were monitored every 20 to 3 months. Computed tomography (CT) or magnetic resonance imaging (MRI) was performed when tumor recurrence was suspected. The patients' clinicopathological characteristics are presented in Table 1. Clinical samples were collected from patients after signing the written informed consent from. The study protocol was approved by the Ethics Committee of the Fifth Affiliated Hospital of Medical School of Nantong University (Taizhou, Jiangsu, China). The tissue samples were all from the biological sample bank of the Fifth Affiliated Hospital of Medical School of Nantong University.

RNA-seq

Total RNA was extracted using the RNeasy Kit (AM1924, Invitrogen), and further treated with DNase to remove genomic DNA contamination. Isolation of mRNA was performed using the NEB. Next PolyA mRNA Magnetic Isolation Module (New England Biolabs, Ipswich, MA, USA) and the mRNA was then used for RNA-Seq library preparation with the NEB Next Ultra Directional RNA Library Prep Kit for Illumina (New England Biolabs, Ipswich, MA, USA). The library was then subjected to Illumina sequencing with paired-end 2x150 as the sequencing mode. Raw reads were filtered to obtain high-quality clean reads by removing sequencing adapters, short reads (length <100 bp) and low-quality reads using Cutadapt (v1.9.1) and Trimmomatic (v0.35). Then Fast QC is used to ensure high reads quality. The clean reads were mapped to the mouse genome (assembly GRCm38) using the HISAT2 software. Gene expression levels were estimated using FPKM (fragments per kilobase of exon per million fragments mapped) by String Tie. Ballgown, a R package, were used to measure differential gene expression. The false discovery rate (FDR) control method was used to calculate the adjusted P-values in multiple testing in order to evaluate the significance of the differences. Here, only gene with an adjusted P-value <0.05 were used for subsequent analysis.

Immunohistochemistry

Tumors were blocked with peroxide and non-immune animal serum and incubated sequentially with indicated first antibodies and biotin-labeled goat anti-rabbit IgG (dilution, 1:1000). Eventually, the tumors were stained with Dolichos biflorus aggultinin (DBA), counterstained with hematoxylin, dehydrated, cleared in xylene, and then fixed. The antibody information is shown in Table S1.

Quantitative reverse transcription polymerase chain reaction (RT-qPCR)

Total RNA was extracted using the RNeasy Kit (AM1924, Invitrogen) according to the manufacturer's instructions, and reversely transcribed into cDNA using AMV reverse transcriptase, which was then used for amplification of the purpose genes. Furthermore, glyceraldehyde 3-phosphate dehydrogenase (GAPDH) was employed as an internal standard. Primer sequences used for RT-qPCR analysis are listed in Table S2.

Cell culture

In the current research, 4 HCC cell lines (Huh-7, MHCC-97H, SMMC-7721, and HepG2) and a normal human liver cell line (LO2) were purchased from the ATCC cell bank. All the cell lines were seeded in 6-well plates at a density of 1.5×10^5 cells/well and maintained in Roswell Park Memorial Institute (RPMI)-1640 (A1049101,Gibco) supplemented with 10% fetal bovine serum (FBS). All the cells were cultured at 37 °C in a humidified atmosphere containing 5% CO2.

Western blot analysis

In the present study, total protein was extracted from cells and tissues subjected to sodium dodecyl sulfate polyacrylamide gel electrophoresis (SDS-PAGE). Protein concentrations were transferred onto polyvinylidene difluoride (PVDF) membranes, and then membranes were blocked and incubated with primary antibody (dilution, 1:1000) at 4 °C overnight. After washing three times with TBS-T solution for 10 min, the membranes underwent hybridization with a goat anti-rabbit IgG secondary antibody (dilution, 1:1000) at 37 °C for 1 h. After further washing, target protein levels were visualized using an enhanced chemiluminescence kit (No. 35055, Thermo Scientific). The antibody information is shown in Table S1.

Transfection

For transfection, the cells were starved 2 h prior to transfection, using Lipofectamine 3000 (L3000015,Invitrogen) on the basis of the manufacturers' protocols. Moreover, at 40 h after transfection, cells were treated with complete media for the indicated period before harvesting for further analysis. The transfection product information are shown in Table S3.

Ionizing radiation (IR) and colony formation

HepG2 cells were seeded into 6-well plates, then exposed to 4 Gy(1 Gy/ min) of X-ray (Rad source, RS2000) and cultured for 48h. Total RNA in the control group and the radiation group were extracted and sequenced. HepG2and Smmc-7721 cells transfected with NC or clone_CLTRN were seeded into 6-well plates, 4Gy for function experiment and ferroptosis detection. Briefly to colony formation, cells were exposed to a range of radiation doses (0, 2, 4, 6 and 8 Gy) and 12 days after irradiation surviving colonies were stained with 0.5% crystal violet and counted. The survival fraction was calculated as the numbers of colonies divided by the numbers of cells seeded times plating efficiency. The plating efficiency was calculated as the ratio of the number of colonies (consisting of at least 50 cells) to the number of seeded cells. The surviving fraction was calculated as the ratio of the plating efficiency of the irradiated cells to that of the non-irradiated ones.

Cell migration and invasion assays.

Cell migration and invasion assays were performed using Millicell Cell Culture Inserts (24-well plates; 8 μm pore size). Stably transduced cells were used for these assays. For the migration assay, cells in serum-free medium were seeded on the upper chambers. For the invasion assays, the membranes of the upper chambers were coated with 8 μl Matrigel (No.A1413301, Gibco) in 32 μl RPMI-1640 medium for 3 h in a humidified incubator. The cells were then seeded in the coated upper chambers. RPMI-1640 medium containing 10% FBS was added into the lower chambers. Cells were incubated for 24 or 48 h for the migration assays, and 48 or 72 h for the invasion assays, respectively. Then, the cells on the lower membranes were stained using a Wright-Giemsa Stain kit (No.9990710, Thermo Scientific) and observed at x100 magnification. Five fields were randomly selected and cells were counted upon observation under a light microscope, the number of cells of average per field was calculated finally.

Apoptosis and cell cycle assay

Cells were trypsinized and centrifuged at 1500 rpm/min for 5 min. Cells were harvested and washed with Phosphate Buffered Saline (PBS) twice. Reagents for apoptosis detection were added, and then cells were incubated in dark for 30 min and subjected to flow cytometry analysis (FACS) (Beckman Coulter, Brea, CA, USA). Additionally, cells were collected, washed with PBS, fixed with 75% ethanol at -20°C overnight, and centrifuged at 1500 rpm/min for 5 min. Then, ethanol was removed and cells were washed with PBS twice. Propidium iodide (PI) and 500 μl of RNAse were added, and then cells were incubated in dark at 4°C for 60 min. Lastly, cells were subjected to cell cycle analysis by FACS.

Animal Studies

A total of 24 BALB/c male nude mice (8 weeks old) were purchased from Shanghai X-B Animal. Ltd(Shanghai, China). All mice were kept in pathogen-free cages in 26-28˚C and 50% humidity. Clone_CLTRN cells and control RNA cells were resuspended in 100 μl PBS and subcutaneously injected into the right side of nude mice ($3x10^6$ cells/mouse, 6 nude mice per group). Next, a 10-Gy dose of IR was delivered to the tumor cell injection site in 9,15days after injection or not. Tumor volumes were measured after 9 days, and every 3 days afterwards. Tumor volume was calculated using the formula: V (mm^3) = width ^{2} (mm^2) x length (mm)/2. All the mice were sacrificed 3 weeks after the injection and tumors were harvested for analysis.

Chromatin immunoprecipitation(CHIP)

Cells were fixed with formaldehyde 1% for 15 min, then cells and nuclei were lysed. The recovered chromatin was sonicated: 10 cycles of 10s (1s on, 1 s off) and precleared. One hundred micrograms chromatin were used for immunoprecipitation with 2 μg of antibodies of NRF1(ab34682, Abcam). Then, the chromatin was incubated with A/G beads for 2h. Crosslinking was reversed by incubation of the beads with SDS at 70°C and proteins were degraded with proteinase K. Finally, DNA was purified using the DNA purification kit (No.142095, CST), and CHIP was analyzed by qPCR using specific primers (Sangon biotech, Shanghai) . Primer sequences are shown in Table S4.

Co-immunoprecipitation (CO-IP)

For the co-immunoprecipitation assay (Co-IP), the cells were lysed with modified TNE buffer (50 mM Tris [pH 8.0], 1% Nonidet P-40 [NP-40], 150 mM NaCl, 2 mM EDTA, 10 mM sodium fluoride, 10 mM sodium pyrophosphate) supplemented with 1 mg/L aprotinin, 1 mM sodium orthovanadate (Na_3VO_4) and 1 mg/L leupeptin. Lysates were centrifuged and cleared by incubation with 25 μl of Protein A/G gel for 1.5 hr at 4°C. The pre-cleared supernatant was subjected to IP using the indicated first antibodies at 4°C overnight. Then, the protein complexes were collected by incubation with 30 μl of Protein A/G gel for 2 hr at 4°C. The protein complexes were resolved by SDS-PAGE. Subsequently, western blot was performed. The antibody information is shown in Table S1.

Coomassie Bright Blue staining and mass spectrum identification

The immunoprecipitation and SDS-PAGE electrophoresis procedures were the same as those for co-immunoprecipitation. The adhesive was placed in a glass dish, Coomassie Bright Blue solution was added, the solution was incubated at 70 °C for 5 min and placed on a shaker for 30 min. The Coomassie Bright Blue solution was then recycled, the adhesive was rinsed with clean water, the Coomassie Bright Blue decolorizing agent was added, and the solution was incubated overnight in a decolorizing shaker. The decolorizing liquid was removed and the adhesive was rinsed with clean water and recovered for using with the target strip. A protein gel recovery kit (No.C500062-0020, Sangon Biotech) was used to recover the target protein. Detection and identification were conducted using mass spectrometry.

Reactive oxygen species (ROS) assay

After trypsin digestion, the cells were washed with PBS and the number of cells was adjusted to 1×10 – 6-2×10^8 cells. DCFH-DA was diluted with serum-free medium at a 1:1000 ratio to a final concentration of 10 μmol/L. To each tube of the sample, 1 mL of the staining solution was added, and the suspension was incubated at 37 °C for 20 min with upside-down mixing every 3-5 min to establish complete contact between the probe and the cells. The cells were washed with PBS and observed using flow cytometry.

Transmission electron microscopy

After the culture medium was discarded, the electron microscope fixator was added and the cells were incubated for 2-4 h at 4 ºC. The cells were centrifuged at a low speed to precipitate them to the bottom of the tube, and cells in the size of mung beans were observed. The cell pellets were wrapped in 1% agarose and rinsed thrice with 0.1 M phosphate buffer (PB, pH 7.4), for 15 min in each round. Next, 1% osmium in 0.1 M PB (pH 7.4) were used to fix the cells at room temperature (20 ºC) and the culture was maintained for 2 h, followed by rinsing with PB (pH 7.4) thrice for 15 min in each round. The tissues were successively dehydrated with 50-70-80-90-95-100-100% alcohol-100% acetone -100% acetone, for 15 min at each step. The following sequential treatment protocol was adopted for the cells: acetone: 812 embedding agent at 1:1 ratio for 2-4 h; acetone: 812 embedding agent at 1:2 ratio, allowed to permeate overnight; treatment with pure 812 embedding agent for 5-8 h. The pure 812 embedding agent was then transferred to the embedding plate, and the sample was placed on the embedding plate and incubated overnight at 37 ºC. Embedment, sectioning, uranium lead double staining followed after this step, after which the samples were observed under a transmission electron microscope.

Iron Assay

The relative iron concentration in cell lysates was assessed using the Iron Assay Kit (No. E-BC-K139-M; Elabscience) according to the manufacturer's instructions.

Immunofluorescence

Cells were grown on poly-L-lysine-coated glass coverslips (BD Biosciences, San Jose, CA), and then fixed with 4% paraformaldehyde, and permeabilized with PBS containing 0.1% Triton X-100 (PBS-T). Coverslips

were incubated in blocking solution containing 2% BSA in PBS for 1 h, and incubated with the appropriate primary RAN and DLD antibody for 1 h at room temperature. After incubation with Alexa Fluor 594-conjugated (red) goat anti-rabbit secondary antibody, cells were stained with DAPI for nuclear staining and then visualized by fluorescence microscopy. The antibody information is shown in Table S1.

Statistical analysis

In the present research, SPSS 19.0 software (IBM, Armonk, NU, USA), GraphPad Prism 6.0 software (GraphPad Software, La Jolla, CA) and R3.6.1 (AT&T Bell Laboratories, USA) were used to perform statistical analyses. Quantitative data were expressed as mean ± standard deviation (SD), and were examined by independent sample t-test. The counting data were analyzed by chi-square test. The Kaplan-Meier estimator was used to estimate the patients' overall survival rates. $P<0.05$ was considered statistically significant.

Results

Results of RNA-seq and identification of target genes

In this study, we studied three pairs of genes from HCC cells and paracancer tissues (BioProject:PRJNA642330)(FigS1A-B). A search in the GEO database yielded 23 pairs of raw data, and not transcripts, under the project PRJNA576155. The cumulative distribution curve from the analysis indicated that the difference was highly consistent[9](Fig1A, FigS1C, E). In addition, we analyzed the changes in protein-coding genes at the transcription level in HepG2 cells before and after X-ray irradiation(BioProject:PRJNA642330) (Fig1B, FigS1D). We screened data based on the following conditions: 1. Upregulated expression in HCC specimens and downregulated expression in cell lines after X-ray irradiation; 2. Downregulated genes in HCC specimens and upregulated genes in cell lines; 3. Q value ranks of the top 30 genes in both groups. Thirteen genes were obtained, and we studied these to further identify the gene of interest in this study(Fig1C-D). We used the QPCR method to analyze transcription level changes in the 13 genes from HepG2 cells before and after X-ray irradiation, and eventually selected CLTRN as the gene of interest, based on the fact that it had undergone the most significant changes(Fig2A).

CLTRN is expressed at low levels in HCC cell lines and tissues, and inhibition of CLTRN expression is associated with poor survival in HCC

The database revealed that CLTRN is primarily localized to the membrane in HCC cells, and we verified the same in HepG2 cells (Fig2B). Thirty cases of paired HCC tumor and paracancer tissue samples were selected to study the expression levels of CLTRN in each tissue sample using RT-qPCR. The results indicated that the expression level of CLTRN in tumor tissues was significantly lower than that in normal tissues (Fig2D). In addition, huh-7, mhcc-97h, smmc-7721, HepG2, and the normal stem cell line LO2 were selected for the analysis of CLTRN expression levels. We observed that the expression level of CLTRN in tumor cells was lower than that in normal cells, particularly in HepG2 cells (Fig2C).The expression levels

of CLTRN in 109 tumor tissues from selected biobanks were analyzed using RT-PCR and accordingly, the samples were categorized into high expression and low expression groups according to the median value. Kaplan-Meier analysis revealed that low expression levels of CLTRN corresponded to poorer survival and higher probability of recurrence (Fig2E-F). In the current study, the Cox proportional-hazards model was used to analyze the clinical data and prognosis in HCC patients. We determined the expression level of CLTRN, TNM staging, and vascular invasion to be independent clinical predictors of survival in HCC, whereas tumor encapsulation, LRRN3 expression, and vascular invasion were independent clinical predictors of recurrence time in HCC (Table 2).

CLTRN overexpression can increase the radiosensitivity of HCC cells in vitro

To investigate the effect of CLTRN on radiosensitivity in HCC cells, HepG2 and SMMC-7721 cells were transfected with negative control (NC) or clone_CLTRN (Fig3A). We observed that high expression of CLTRN was associated with reduced survival fraction (SF) in HCC cells with IR(Fig3B). The migration and invasion experiments also revealed that the overexpression of CLTRN could reduce the migration and invasive potential of HCC cells after treatment with IR(Fig3C-D). However, overexpression of CLTRN did not significantly affect the cell cycle and apoptosis of HCC cells after treatment with IR (Fig3E-F).

CLTRN overexpression can reduce tumorigenicity in nude mice post-irradiation

HepG2 cells with stable overexpression of CLTRN were established for studying in vivo tumorigenesis in nude mice. We randomly divided 24 nude mice into four groups, namely NC, clone_CLTRN, NC+IR, and clone_CLTRN+IR. The tumor was treated using radiation during tumor growth, and the tumor formation potential in each group was compared. We observed that the tumor volume was the lowest in nude mice that were treated with radiation after CLTRN overexpression, which indicates that CLTRN overexpression could enhance the radiosensitivity of HCC cells (Fig4A-C).

CLTRN is primarily associated with glutathione metabolism in HCC cells.

We used RNA-seq to analyze the changes in protein-coding genes at the transcription level induced upon CLTRN overexpression in HepG2 cells (BioProject:PRJNA642330)(Fig5A-B). Combining our data with those from KEGG database and bioinformatics analyses, we observed that the altered genes were mostly enriched in the glutathione metabolic pathway (Fig5C). We hypothesized that CLTRN might be associated with glutathione metabolism.

CLTRN overexpression can increase ferroptosis in HCC, and CLTRN can enhance the radiosensitivity of HCC cells through the ferroptosis pathway.

Since glutathione metabolism is a key mechanism in ferroptosis, we further hypothesized that CLTRN could play a role in the ferroptosis pathway (Fig5D)[10]. We performed the relevant validation experiments in HepG2 and SMCC-7721 cells. The cells were divided into the following three groups: NC, NC+IR, and clone_CLTRN+IR. The concentration of iron ions in the cell lysate and the levels of ROS in the liposomes were studied. Lastly, the changes in the organelles in each group were observed using

transmission electron microscopy. We found that radiation could independently induce an increase in the concentration of cellular iron ions and could also increase the levels of ROS in cellular liposomes (Fig6A-B), which suggests that radiation can induce ferroptosis in HCC. The results of transmission electron microscopy also revealed that the number of mitochondria decreased, their membrane density increased, and the number of cristae in mitochondria decreased in cells from the NC+IR group (Fig6C); however, compared to the cells from the NC+IR group, the radiosensitivity of tumor cells increased significantly upon the overexpression of CLTRN (Fig6C). The above experimental results indicated that CLTRN enhanced the radiosensitivity of tumor cells by increasing ferroptosis. Furthermore, we compared the changes in the expression of protein indicators associated with glutathione metabolism and ferroptosis, including glutathione peroxidase 4 (GPX4), solute carrier family 7 member 11 (SLC7A11), ferritin, heavy polypeptide 1 (FTH1), prostaglandin endoperoxide synthase 2 (PTGS2), NADPH oxidase 1 (NOX1), and acyl-CoA synthetase long-chain family member 4 (ACSL4), after CLTRN overexpression. The results indicated that PTGS2, NOX1, and ACSL4 were upregulated, while GPX4, SLC7A11, and FTH1 were downregulated in cells that overexpressed CLTRN, which further confirmed the function of CLTRN in the ferroptosis pathway and its effect on the proliferation of tumor cells (Fig6D). Moreover, the levels of GPX4 and SLC7A11 expression were also the lowest in the clone_CLTRN+IR group, as observed from the immunohistochemical sections of tissue samples from nude mice, which indicates that ferroptosis was most pronounced in this group (Fig4D).

NRF1 is a transcription factor and upstream regulator of CLTRN.

We further investigated the upstream regulatory mechanism of CLTRN. Bedtools was used to extract the sequences 1500 bp upstream and 500 bp downstream of the transcription start site to predict the transcription factor binding site on the JASPAR website. Eleven candidate transcription factors were obtained at $p < 0.01$ (Fig7A). We determined the RNA expression levels of these 11 candidate transcription factors in HCC and paracancer specimens, and observed that YY1 transcription factor (YY1), HNF1 homeobox A (HNF1A), paired box 5 (PAX5), and NRF1 were downregulated in the tumor and upregulated in paracancer tissues, which was also consistent with the expression pattern of CLTRN (Fig7B). Subsequently, interfering sequences were designed for these four genes and the interference was implemented successfully in HepG2 cells. Western blot analysis of the interfering proteins and CLTRN was conducted in each group. The results indicated that CLTRN expression reduced significantly only upon interference with NRF1, which indicates that NRF1 might be the upstream transcription factor of CLTRN (Fig7C-E). We then collected the chip-SEQ data of NRF1 in HepG2 cells (GEO:GSE96424) and analyzed the binding DNA, and found that CLTRN was one of its binding DNA sequences (Fig7G). Using chip-QPCR, we finally confirmed the binding between NRF1 and CLTRN at the site predicted by the software (Fig7F,H).

Member RAS oncogene family (RAN) and Dihydrolipoamide dehydrogenase (DLD)are interacting proteins of NRF1 in HCC cells

We attempted to identify the interaction proteins of NRF1 in HCC. We used HepG2 cells as the research object and performed immunoprecipitation with an NRF1 antibody. After Coomassie Blue staining, the samples were electrophoresed, the corresponding fragments were cut out from the gel, and mass spectrometry analysis was conducted (Fig8A-B). For the top 100 proteins obtained using mass spectrometry, we conducted correlation screening in the GEPIA database and selected proteins with R values > 0.3. We attempted to determine the location of these proteins from the UniProt database, selected the nucleus-localized proteins, and identified RAN and DLD as the target proteins (Fig8C-D). The immunofluorescence assay revealed that RAN and DLD were indeed located in the nuclei of HepG2 cells (Fig8E). Finally, in the co-immunoprecipitation experiment, we confirmed that RAN and DLD are the interacting proteins of NRF1 (Fig8F).

Discussion

HCC is one of the most common and aggressive malignancies with global prevalence, and ranks sixth in terms of the number of cases and third in terms of cancer mortality[11, 12]. Since most patients with HCC do not exhibit specific symptoms at an early stage, the proportion of patients with resectable HCC is low. Non-surgical treatment is of great importance for patients with HCC who cannot undergo surgical resection. Radiotherapy is an important non-surgical treatment method for cancer; however, its clinical application is limited owing to the prevalence of radiotherapy resistance in patients. Therefore, we primarily focused on methods for improving radiosensitivity in HCC cells.

Here, we first used RNA-seq technology to study the upregulated genes in HCC tissue chips, along with the genes with altered expression after radiation treatment of HepG2 cells, and found 13 genes that may be associated with HCC radiosensitivity, which was subsequently verified. We concluded that CLTRN may function as a HCC radiosensitivity gene.

The collectrin gene (CLTRN, Gene Bank ID:AF178085), also known as Tmem27, was first isolated and cloned from kidney tissues in 1999[13]. CLTRN is a type Ia transmembrane glycoprotein located in the cell membrane and is highly conserved among species[14, 15]. In mice, collectrin deficiency causes profound aminoaciduria involving both neutral and charged amino acids[16]. The expansion in the biochemical phenotype over that seen in Hartnup disease is thought to be associated with the additional role played by collectrin in the functioning of other renal amino acid transporters[17].

Currently, there are a limited number of studies on the function of CLTRN, and the major findings are related to its role in the regulation of arterial pressure, nervous system, and blood glucose levels[17–19]. CLTRN has also been studied inextensively in tumors (only in kidney cancer)[20]. In this study, we observed that CLTRN can inhibit invasion, migration, and proliferation of HCC cells after irradiation in vitro, which suggests that CLTRN is associated with the biological behavior of liver cancer cells. However, CLTRN did not exert significant effect on the cell cycle and apoptosis of HCC cells. In vivo tumor formation in nude mice also revealed that CLTRN could alter the effect of radiation on tumor formation in nude mice, and when overexpressed, it could improve the sensitivity of tumors to radiation.

CLTRN is associated with tumor biological behavior in HCC; however, the mechanism underlying the regulation of HCC cells by CLTRN remains unclear. We observed that CLTRN was overexpressed in HepG2 cells, and transcriptional-level changes of the protein-coding genome of the overexpressed and control cells were analyzed using RNA-sEq. KEGG pathway analysis of the transcriptome data revealed that CLTRN was significantly associated with glutathione metabolism. Glutathione is widely found in animals and plants and plays an important role in organisms. Furthermore, glutathione metabolism has been linked to ferroptosis.

Ferroptosis, an iron-dependent form of programmed cell death that is induced by excessive lipid peroxidation, is morphologically and mechanistically distinct from apoptosis[21–23]. GPX4, a type of glutathione peroxidase, utilizes reduced glutathione to convert lipid hydroperoxides to lipid alcohols, and thereby mitigates lipid peroxidation and inhibits ferroptosis[24–26]. The amino acid transporter SLC7A11 (also known as xCT) assists in the delivery of extracellular cysteine into the cell[27, 28]. Resultantly, the inactivation of GPX4 or SLC7A11 through genetic or pharmacologic means induces ferroptosis. Recent studies have revealed that FSP1 plays an important role in ferroptosis. A protein similar to other Ufm1-specific proteases (FSP1), a CoQ oxidoreductase, plays a role similar to GPX4 during ferroptosis and has been denoted as a new ferroptosis effector protein, similar to GPX4[29, 30].

We hypothesized that CLTRN is associated with ferroptosis and influences the tumor biology of HCC cells through ferroptosis. We investigated whether CLTRN overexpression causes biological changes in cell-associated ferroptosis. The results indicated that the cytoplasm of HepG2 cells that overexpress CTLRN underwent significant changes in ferroptosis morphology after IR. In addition, compared to the blank control cells, the IR cells also exhibited certain signs of ferroptosis, which suggests that radiation could independently cause ferroptosis in tumor cells. Recent studies have revealed that IR induces ROS generation as well as the expression of ACSL4, which is an lipid metabolic enzyme essential for ferroptosis, and consequently increases lipid peroxidation and ferroptosis. ACSL4 deficiency can largely eliminate IR-induced ferroptosis and enhance radiation resistance[31]. At the protein level, after the overexpression of CLTRN, the expression levels of index proteins associated with glutathione metabolism and ferroptosis alteredsignificantly, which further indicates that CLTRN plays a role in enhancing the radiosensitivity of tumor cells through glutathione metabolic-ferroptosis pathway.

We identified NRF1 as the upstream regulatory transcription factor of CLTRN using database prediction and verification. NRFl is a transcription factor encoded by nuclear genes, which regulates the expression of mitochondrial respiratory chains[32]. NRF1 induces the expression of the protein components of the mitochondrial respiratory chain, regulates the expression of mitochondrial transport proteins and mitochondrial oxidative stress-related proteins, and participates in estrogen-mediated mitochondrial biosynthesis and cellular metabolism[33]. NRF1 is associated with the incidence and development of breast cancer, and its dynamic transcriptional regulation patterns can be studied to predict cancer risk and efficacy [34]. Our study is the first to demonstrate that NRF1 affects the ferroptosis network of cells by regulating CLTRN expression in liver cancer. We predicted Ran and DLD to be the interacting proteins using immunoprecipitation-mass spectrometry in combination with database analysis, and verified the

same in co-immunoprecipitation experiments. RAN is a GTPase associated with the RAS family and encodes the Ras-related nuclear protein, which is a unique member of the Ras superfamily of GTPases[35]. Mutations in the RAN gene likely play a critical role in pathology-related changes in miRNA transport and expression, and therefore, contribute to tumorigenesis and development[36]. DLD is associated with cysteine metabolism and regulation of ROS generation[37], and its role in tumor growth regulation mediated through the ferroptosis pathway in neck tumors has been investigated[38]. We observed that DLD and RAN regulate CLTRN expression in HCC cells by interacting with NRF1, and thereby affect ferroptosis and enhance the radiosensitivity of HCC cells.

Conclusion

To summarize, we identified a novel HCC radiosensitivity gene and investigated its upstream and downstream regulatory mechanisms. CLTRN, which is regulated by the NRF1/RAN/DLD protein complex, enhances the radiosensitivity of HCC cells through ferroptosis (Fig. 8G).

Abbreviations

HCC: hepatocellular carcinoma cells; CLTRN:collectrin; NRF1:nuclear respiratory factor 1; RNA:RAS oncogene family; DLD:dihydrolipoamide dehydrogenase; PARP-1:poly (ADP-ribose) polymerase 1; PKCε:protein kinase C, epsilon; ZEB1:zinc finger E-box binding homeobox 1; GAPDH:glyceraldehyde 3-phosphate dehydrogenase; FACS:flow cytometry analysis; CHIP:Chromatin immunoprecipitation; CO-IP:co-immunoprecipitation; ROS:reactive oxygen species; GPX4:glutathione peroxidase 4; SLC7A11:solute carrier family 7 member 11; FTH1:ferritin, heavy polypeptide 1; PTGS2:prostaglandin endoperoxide synthase 2; NOX1:NADPH oxidase 1; ACSL4:acyl-CoA synthetase long-chain family member 4; YY1:YY1 transcription factor; HNF1A:HNF1 homeobox A; PAX5:paired box 5; FSP1:Ufm1-specific proteases;

Declarations

Acknowledgements

We are very grateful to Dr. Wang HG, the Department of General surgery of the Fifth Affiliated Hospital of Medical School of Nantong University, Taizhou, China for bioinformatics analyses and funding support. We would like to thank Editage (www.editage.cn) for English language editing.

Funding

This work was supported by grants from the Fifth Affiliated Hospital of Medical School of Nantong University, Taizhou, China (ZL201817); the National Natural Science Foundation of China (Grant 81600434); Natural Science Foundation of Jiangsu Province (Grants BK 20160572 and BK 20170358);Jiangsu Provincial Medical Youth Talent (Grant QNRC 2016514);and China Postdoctoral Science Foundation (Grant 2018M630581).

Availability of data and materials

All data generated or analyzed during this study are included in this published article and its supplementary information files.

Authors' contributions

YY and QHX designed experiments and wrote the paper; YY, WHG, ZHB and CW performed experiments and provided technical support. All authors read and approved the final manuscript.

Ethics approval and consent to participate

This study was reviewed and approved by the ethics committee of the

Fifth Affiliated Hospital of Medical School of Nantong University. All experiments involving laboratory animals followed the Guidelines for Animal Experiments of the Fifth Affiliated Hospital of Medical School of Nantong University.

Consent for publication

Not applicable.

Competing interests

The authors declare that they have no competing interests.

References

1. Torre LA, Bray F, Siegel RL, Ferlay J, Lortet-Tieulent J, Jemal A. Global cancer statistics, 2012. CA Cancer J Clin. 2015;65(2):87–108.
2. Chen W, Zheng R, Baade PD, Zhang S, Zeng H, Bray F, et al. Cancer statistics in China, 2015. CA Cancer J Clin. 2016;66(2):115–32.
3. El-Serag HB. Hepatocellular carcinoma. N Engl J Med. 2011;365(12):1118–27.
4. Tanguturi SK, Wo JY, Zhu AX, Dawson LA, Hong TS. Radiation therapy for liver tumors: ready for inclusion in guidelines. Oncologist. 2014;19(8):868–79.
5. Stark TW, Hensley PJ, Spear A, Pu H, Strup SS, Kyprianou N. Predictive value of epithelial-mesenchymal-transition (EMT) signature and PARP-1 in prostate cancer radioresistance. Prostate. 2017;77(16):1583–91.
6. El Bezawy R, Tinelli S, Tortoreto M, Doldi V, Zuco V, Folini M, et al. miR-205 enhances radiation sensitivity of prostate cancer cells by impairing DNA damage repair through PKCε and ZEB1 inhibition. J Exp Clin Cancer Res. 2019;38(1):51.

7. Shao Y, Song X, Jiang W, Chen Y, Ning Z, Gu W, et al. MicroRNA-621 Acts as a Tumor Radiosensitizer by Directly Targeting SETDB1 in Hepatocellular Carcinoma. Mol Ther. 2019;27(2):355–64.
8. Yang X, Liu W, Xu X, Zhu J, Wu Y, Zhao K, et al. Downregulation of long non–coding RNA UCA1 enhances the radiosensitivity and inhibits migration via suppression of epithelial–mesenchymal transition in colorectal cancer cells. Oncol Rep. 2018;40(3):1554–64.
9. Shi H, Liu C, Tan H, Li Y, Nguyen TM, Dhungana Y, et al. Hippo Kinases Mst1 and Mst2 Sense and Amplify IL-2R-STAT5 Signaling in Regulatory T Cells to Establish Stable Regulatory Activity. Immunity. 2018;49(5):899–914.e6.
10. Mou Y, Wang J, Wu J, He D, Zhang C, Duan C, et al. Ferroptosis, a new form of cell death: opportunities and challenges in cancer. J Hematol Oncol. 2019;12(1):34.
11. Bray F, Ferlay J, Soerjomataram I, Siegel RL, Torre LA, Jemal A. Global cancer statistics 2018: GLOBOCAN estimates of incidence and mortality worldwide for 36 cancers in 185 countries. CA Cancer J Clin. 2018;68(6):394–424.
12. Lee WC, Lee CF, Cheng CH, Wu TJ, Chou HS, Wu TH, et al. Outcomes of liver resection for hepatocellular carcinoma in liver transplantation era. Eur J Surg Oncol. 2015;41(9):1144–52.
13. Zhang H, Wada J, Kanwar YS, Tsuchiyama Y, Hiragushi K, Hida K, et al. Screening for genes up-regulated in 5/6 nephrectomized mouse kidney. Kidney Int. 1999;56(2):549–58.
14. Akpinar P, Kuwajima S, Krützfeldt J, Stoffel M. Tmem27: a cleaved and shed plasma membrane protein that stimulates pancreatic beta cell proliferation. Cell Metab. 2005;2(6):385–97.
15. Zhang H, Wada J, Hida K, Tsuchiyama Y, Hiragushi K, Shikata K, et al. Collectrin, a collecting duct-specific transmembrane glycoprotein, is a novel homolog of ACE2 and is developmentally regulated in embryonic kidneys. J Biol Chem. 2001;276(20):17132–9.
16. Malakauskas SM, Quan H, Fields TA, McCall SJ, Yu MJ, Kourany WM, et al. Aminoaciduria and altered renal expression of luminal amino acid transporters in mice lacking novel gene collectrin. Am J Physiol Renal Physiol. 2007;292(2):F533-44.
17. Pillai NR, Yubero D, Shayota BJ, Oyarzábal A, Ghosh R, Sun Q, et al. Loss of CLTRN function produces a neuropsychiatric disorder and a biochemical phenotype that mimics Hartnup disease. Am J Med Genet A. 2019;179(12):2459–68.
18. KOlakovic A, Zivkovic M, Djuric T, Koncar I, Stankovic A. The expression of renin-angiotensin-system components (ACE, ACE2 and collectrin (TMEM27)) in the human carotid plaques depending on gender and plaque phenotype. Atherosclerosis. 2018;275(1):135.
19. Pepaj M, Gjerlaugsen N, Julien K, Thorsby PM. Tmem27 is upregulated by vitamin D in INS-1 cells and its serum concentrations are low in patients with autoimmune diabetes. Scand J Clin Lab Invest. 2014;74(4):358–65.
20. Javorhazy A, Farkas N, Beothe T, Pusztai C, Szanto A, Kovacs G. Lack of TMEM27 expression is associated with postoperative progression of clinically localized conventional renal cell carcinoma. J Cancer Res Clin Oncol. 2016;142(9):1947–53.

21. Dixon SJ, Lemberg KM, Lamprecht MR, Skouta R, Zaitsev EM, Gleason CE, et al. Ferroptosis: an iron-dependent form of nonapoptotic cell death. Cell. 2012;149(5):1060–72.
22. Stockwell BR, Friedmann Angeli JP, Bayir H, Bush AI, Conrad M, Dixon SJ, et al. Ferroptosis: A Regulated Cell Death Nexus Linking Metabolism, Redox Biology, and Disease. Cell. 2017;171(2):273–85.
23. Gao M, Jiang X. To eat or not to eat-the metabolic flavor of ferroptosis. Curr Opin Cell Biol. 2018;51:58–64.
24. Seibt TM, Proneth B, Conrad M. Role of GPX4 in ferroptosis and its pharmacological implication. Free Radic Biol Med. 2019;133:144–52.
25. Friedmann Angeli JP, Schneider M, Proneth B, Tyurina YY, Tyurin VA, Hammond VJ, et al. Inactivation of the ferroptosis regulator Gpx4 triggers acute renal failure in mice. Nat Cell Biol. 2014;16(12):1180–91.
26. Yang WS, SriRamaratnam R, Welsch ME, Shimada K, Skouta R, Viswanathan VS, et al. Regulation of ferroptotic cancer cell death by GPX4. Cell. 2014;156(1–2): 317 – 31.
27. Koppula P, Zhang Y, Zhuang L, Gan B. Amino acid transporter SLC7A11/xCT at the crossroads of regulating redox homeostasis and nutrient dependency of cancer. Cancer Commun (Lond). 2018;38(1):12.
28. Conrad M, Sato H. The oxidative stress-inducible cystine/glutamate antiporter, system x (c) (-): cystine supplier and beyond. Amino Acids. 2012;42(1):231–46.
29. Doll S, Freitas FP, Shah R, Aldrovandi M, da Silva MC, Ingold I, et al. FSP1 is a glutathione-independent ferroptosis suppressor. Nature. 2019;575(7784):693–8.
30. Bersuker K, Hendricks JM, Li Z, Magtanong L, Ford B, Tang PH, et al. The CoQ oxidoreductase FSP1 acts parallel to GPX4 to inhibit ferroptosis. Nature. 2019;575(7784):688–92.
31. Lei G, Zhang Y, Koppula P, Liu X, Zhang J, Lin SH, et al. The role of ferroptosis in ionizing radiation-induced cell death and tumor suppression. Cell Res. 2020;30(2):146–62.
32. Scarpulla RC, Gopalakrishnan L. Structure, expression, and chromosomal assignment of the human gene encoding nuclear respiratory factor 1. J Biol Chem. 1995;270(30):18019–25.
33. Klinge CM. Estrogens regulate life and death in mitochondria. J Bioenerg Biomembr. 2017;49(4):307–24.
34. Roy D, Bhawe K. Interplay between NRF1, E2F4 and MYC transcription factors regulating common target genes contributes to cancer development and progression. Cell Oncol (Dordr). 2018;41(5):465–84.
35. Nishimoto T. A new role of ran GTPase. Biochem Biophys Res Commun. 1999;262(3):571–4.
36. Li Y, Zhang F, Xing C. A Systematic Review and Meta-Analysis for the Association of Gene Polymorphisms in RAN with Cancer Risk. Dis Markers. 2020;2020:9026707.
37. Dayan A, Fleminger G, Ashur-Fabian O. Targeting the Achilles' heel of cancer cells via integrin-mediated delivery of ROS-generating dihydrolipoamide dehydrogenase. Oncogene.

2019;38(25):5050–61.
38. Shin D, Lee J, You JH, Kim D, Roh JL. Dihydrolipoamide dehydrogenase regulates cystine deprivation-induced ferroptosis in head and neck cancer. Redox Biol. 2020;30:101418.

Tables

Table 1: Expression of CLTRN by immunohistochemical and clinicopathologic features of HCC patients (n=109)

Variables	Expression of CLTRN		p
	low（56）	high（53）	
Sex			0.50
Female	26	28	
Male	30	25	
Age（y）			0.51
≤51	25	27	
>51	31	26	
Preoperative AFP(ng/mL)			
≤20			0.29
>20		16	
	12	37	
	44		
HBsAg			0.98
Negative	20	19	
Positive	36	34	
Liver cirrhosis			0.87
No	25	19	
Yes	31	34	
Tumor size(cm)			0.63
≤5	24	32	
>5	32	21	
Tumor number			0.10
Single	39	44	
Multiple	17	9	

Tumor encapsulation			0.80
No	33	30	
Yes	23	23	
Vascular invasion			0.002**
No	17	33	
Yes	39	23	
TNM stage			0.004**
I-II	35	35	
III-IV	21	18	
Tumor differentiation			
I-II	24	40	0.0005***
III-IV	32	13	

CLTRN, Collectrin; TNM, tumor, node and metastasis; AFP, alpha-fetoprotein; **p<0.01, ***p<0.001

Table 3 Cox regression analyses of factors associated with OS and TTR of HCC Patients（n=109）

Variables	Overall Survival		Time to Recurrence	
	Hazard ratio(95%CI)	P value	Hazard ratio(95%CI)	P value
Sex (female vs. male)	1.011(0.987-1.034)	0.371	1.014(0.991-1.038)	0.226
Age（Y(≤51 vs.>51)	1.671(0.571-1.504)	0.759	0.797(0.492-1.294)	0.359
Tumor differentiation (III-IV vs. I-II)	2.625(0.629-4.440)	0.303	1.626(0.683-3.870)	0.272
AFP (ng/mL;>20 vs. ≤20)	1.518(0.762-3.023)	0.235	1.019(0.529-1.965)	0.955
HbsAg (Negative vs. Positive)	1.055(0.443-2.513)	0.904	1.099(0.438-2.757)	0.841
Liver cirrhosis (no vs. yes)	0.990(0.463-2.114)	0.978	1.002(0.439-2.288)	0.996
Tumor number (Multiple vs. Single)	1.056(0.405-2.775)	0.911	0.817(0.323-2.064)	0.669
Tumor encapsulation (yes vs. no)	1.131(0.478-2.667)	0.779	2.461(1.248-4.851)	0.009**
Vascular invasion (yes vs. no)	2.034(1.171-3.533)	0.011*	2.233(1.299-3.840)	0.003**
TNM stage (III-IV vs. I-II)	2.493(1.282-4.849)	0.007**	1.491(0.646-3.474)	0.353
CLTRN (high vs. low)	0.393(0.230-0.670)	0.003**	0.406(0.249-0.660)	<0.001***

*, p<0.05; **, p<0.01, *** p<0.001 CLTRN, Collectrin.

Figures

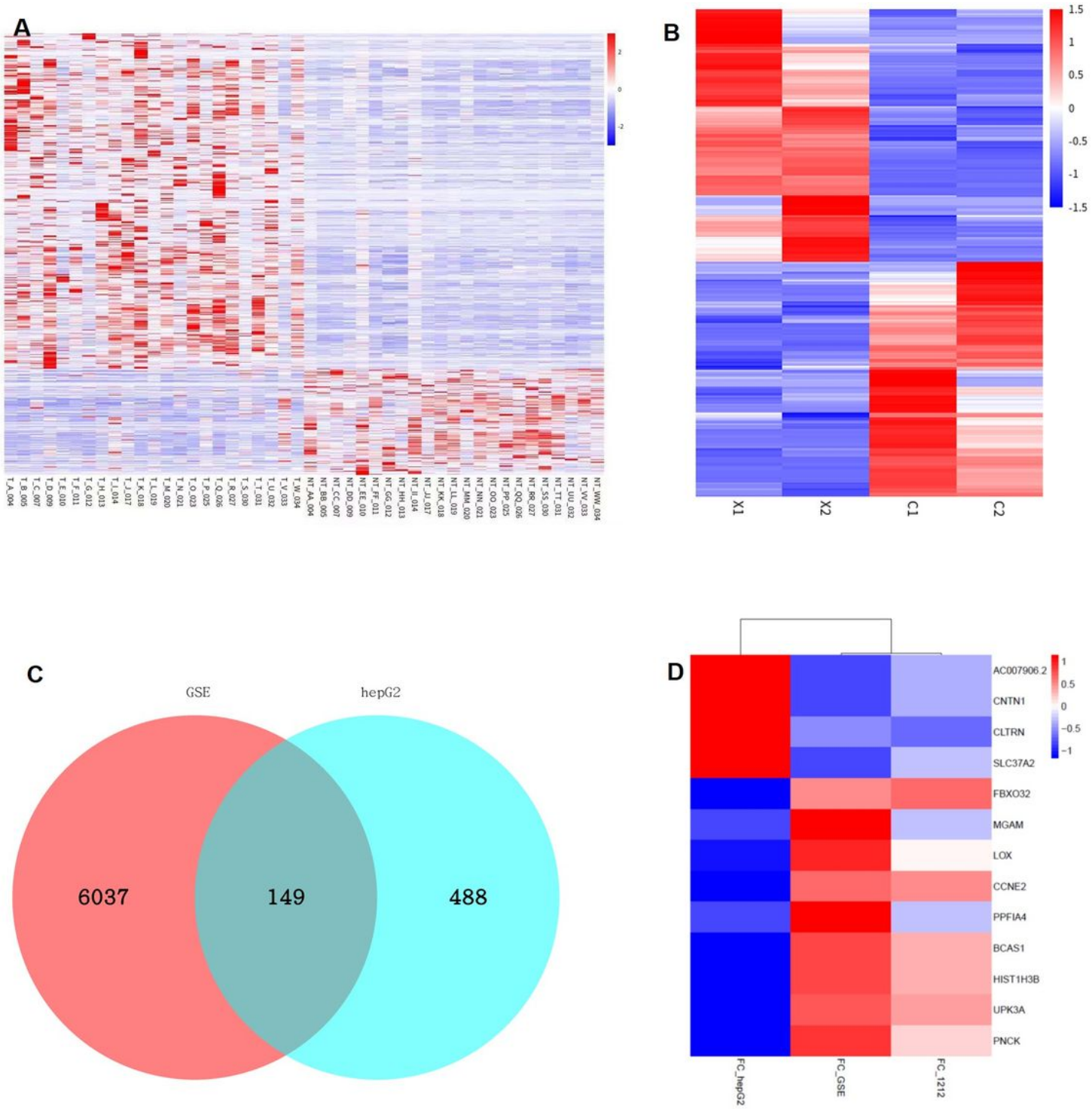

Figure 1

RNA-seq of hepatocellular carcinoma (HCC) tissues and irradiation HCC cells. a Heat maps of HCC and paired paracancer tissues analyzed using RNA-seq. b Heat maps of the Hepg2 cell line before and after irradiation analyzed using RNA-seq. c Venn diagram depicting the upregulation and downregulation of genes with opposing functions in HCC tissues and HepG2 cell lines after irradiation. d Heat map of candidate genes screened according to the parameters.

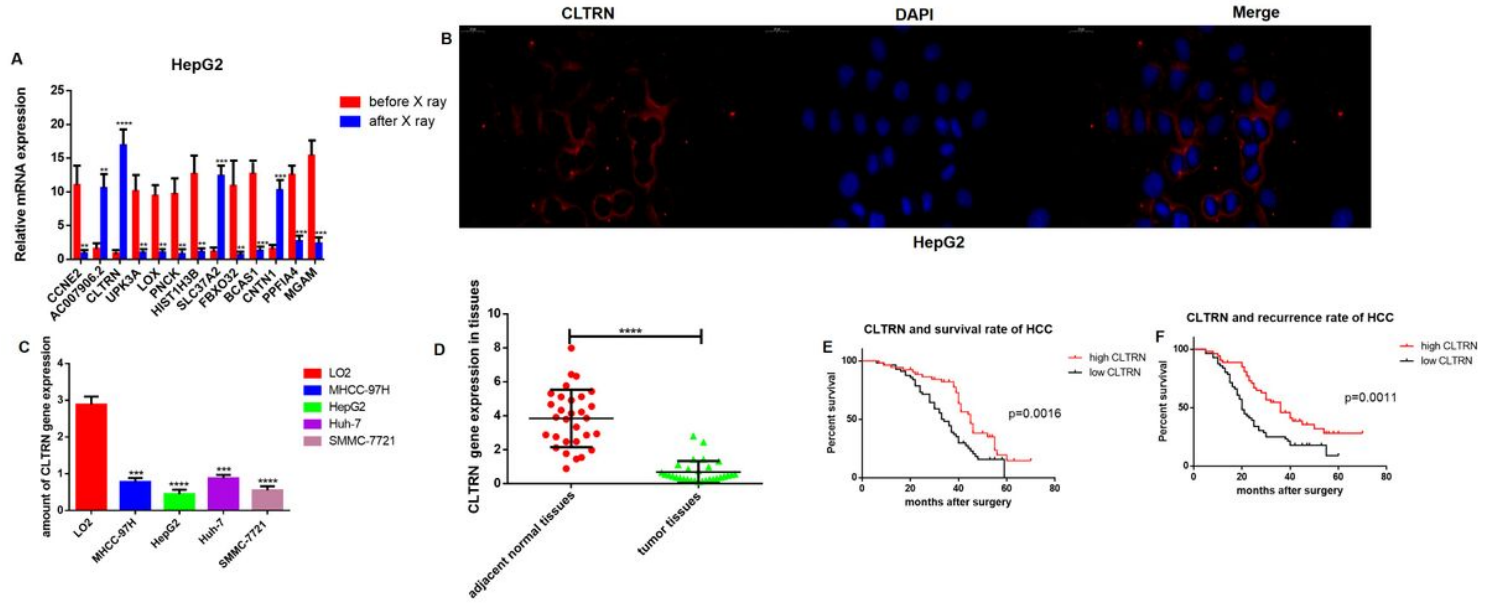

Figure 2

CLTRN is weakly expressed in HCC tissues and cells and is associated with the prognosis in patients with HCC. a RNA expression of the 13 candidate genes before and after HepG2 irradiation was analyzed using QPCR. b CLTRN is primarily localized to the cell membrane in HCC, Scale bars: 20 μm. c CLTRN expression was low in HCC cells. d CLTRN is weakly expressed in HCC tissues. e Low CLTRN expression in HCC patients is associated with a poorer survival prognosis. f Low CLTRN expression in HCC patients suggests earlier recurrence. The data are expressed in terms of mean ± SD (Student's t-test and Kaplan-Meier test ; *** P < 0.001; **** P < 0.0001).

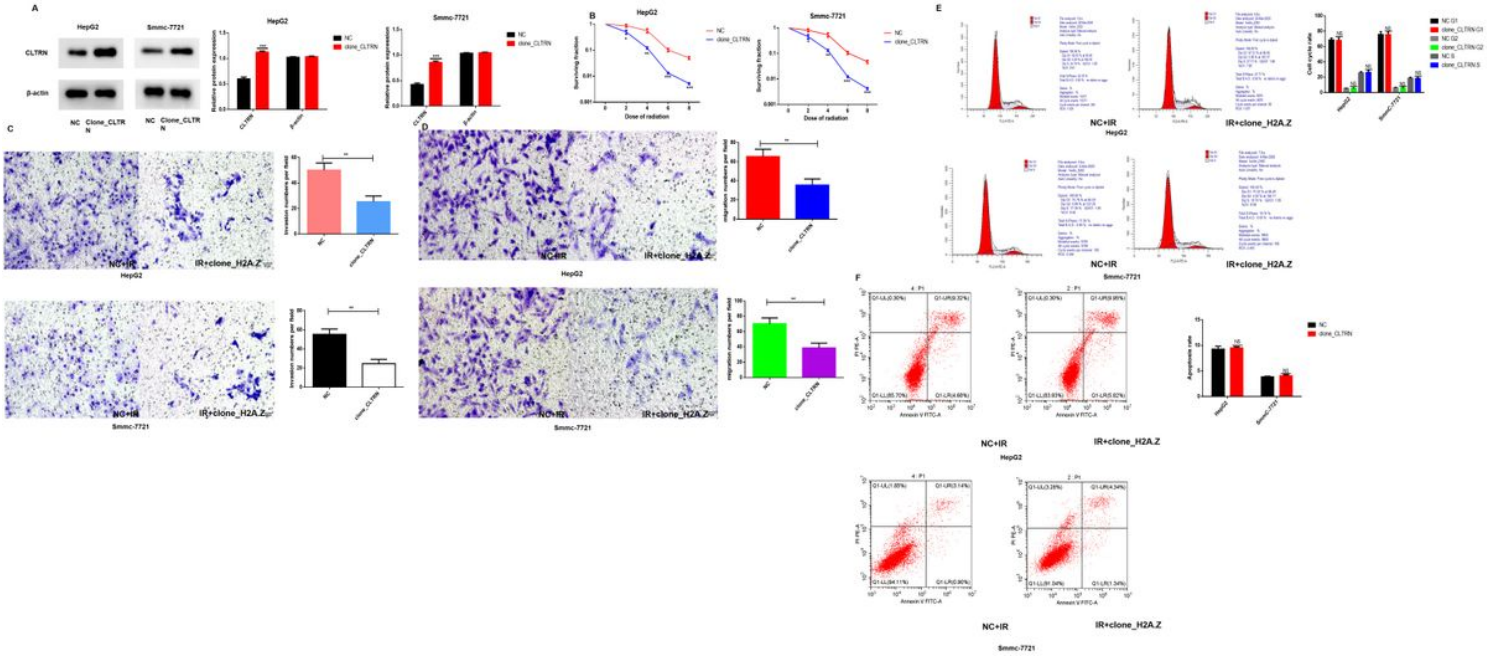

Figure 3

CLTRN overexpression can lead to increased radiosensitivity in HCC cells in vitro. a Identification of the CLTRN transfection effect. b In HepG2 and SMCC-7721 cells that overexpress CLTRN , the cloning potential of the cells decreased upon radiation treatment. c In HepG2 and SMCC-7721 cells that overexpress CLTRN, the invasive potential of cells reduced upon radiation treatment. d In HepG2 and SMCC-7721 cells that overexpress CLTRN, the migration potential of cells reduced upon radiation treatment. e In HepG2 and SMCC-7721 cells that overexpress CLTRN, there was no significant change observed in the apoptosis rate in response to radiation treatment. f In HepG2 and SMCC-7721 cells that overexpress CLTRN, the cell cycle did not undergo significant changes upon radiation treatment. The data are expressed in terms of mean ± SD (Student's t-test; * P < 0.05; ** P < 0.01;*** P < 0.001; NS no significance).

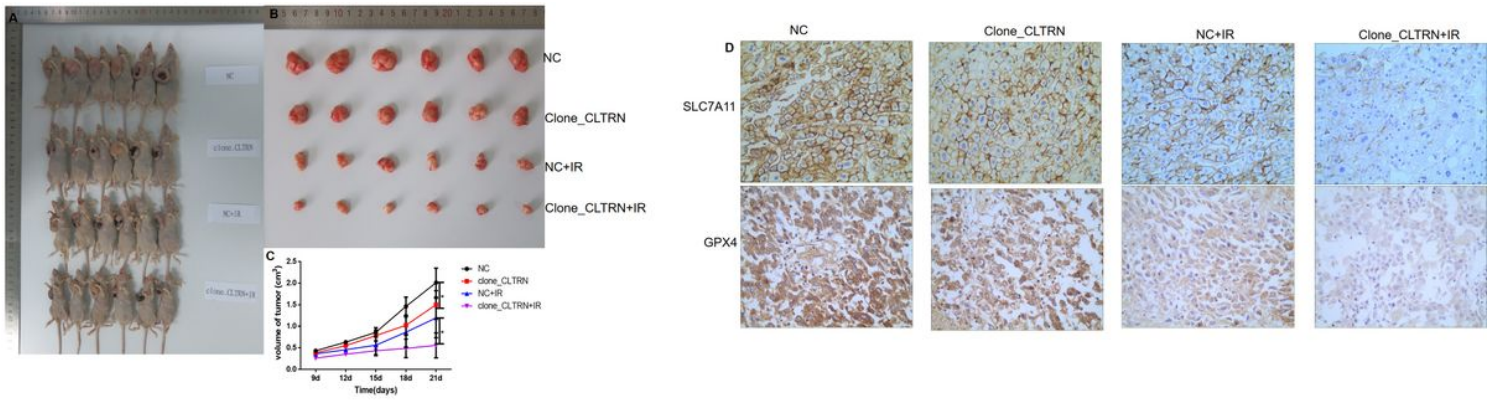

Figure 4

Tumorigenicity in cells that overexpress CLTRN can reduce upon radiation treatment. a General view of tumor formation in different groups of nude mice. b General view of tumors in different groups of nude mice. c Planting growth curve of nude mice from different groups. d Immunohistochemical analysis of GPX4 and SLC7A11 proteins in tumors in nude mice from different groups(Scale bars: 400×). The data are expressed in terms of mean ± SD (Student's t-test; * P < 0.05).

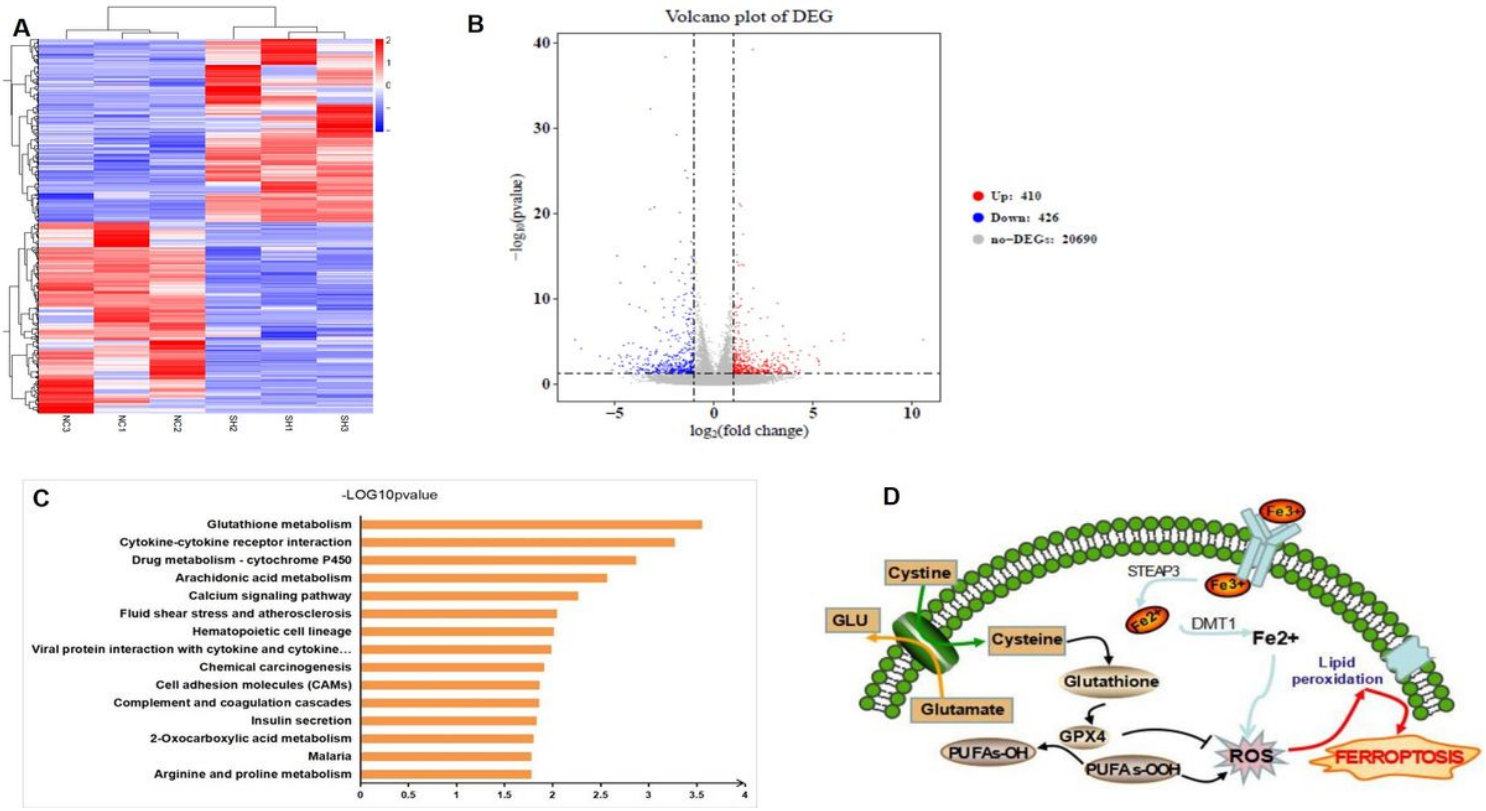

Figure 5

CLTRN may play a role in glutathione metabolism and ferroptosis in liver cancer cells, as determined through RNA-seq analysis. a Heat map of whole-gene transcriptomic changes in HepG2 cells that overexpress CLTRN. b Volcanogram of changes at the whole-gene transcriptomic level in HepG2 cells that overexpress CLTRN. c KEGG pathway analysis was used to analyze the regulatory pathways that CLTRN might be associated with in HCC cells. d Schematic diagram of ferroptosis.

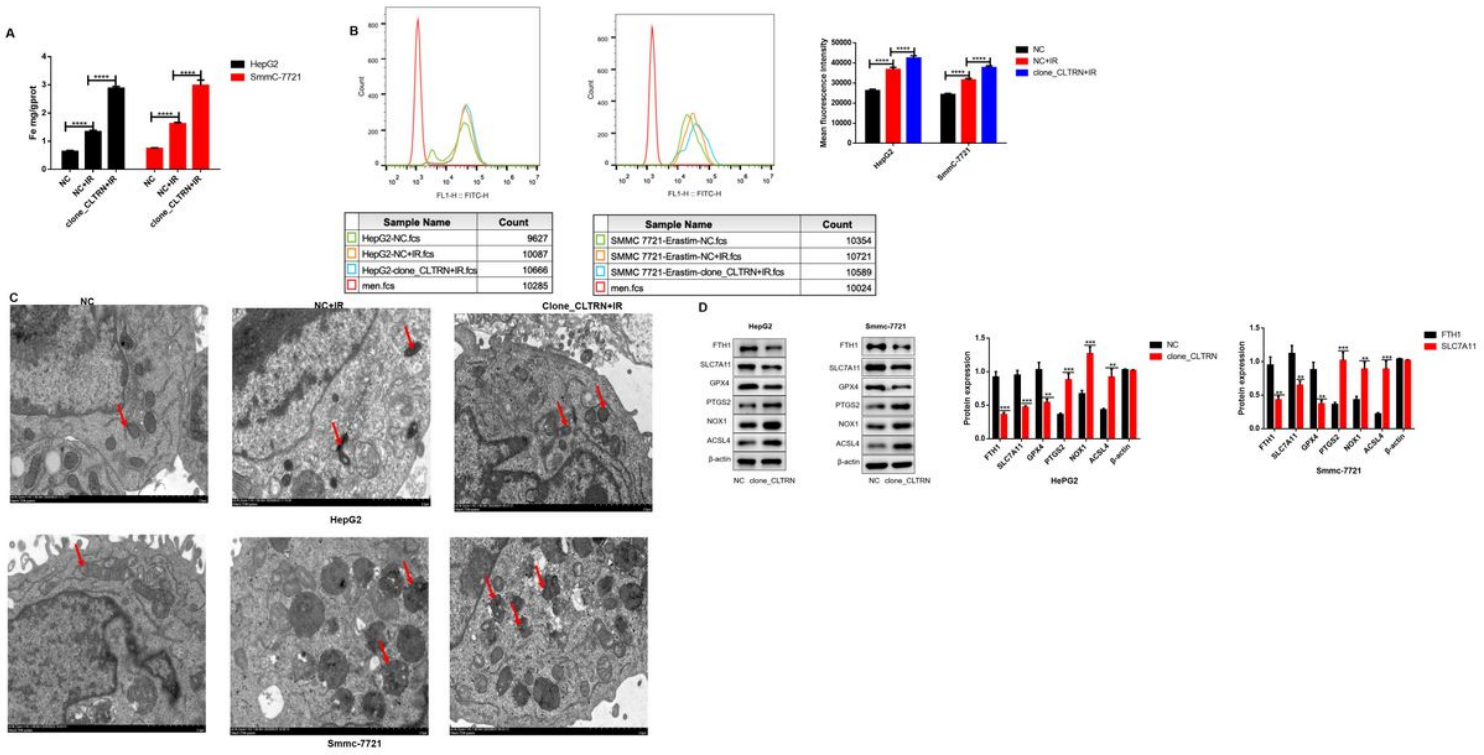

Figure 6

CLTRN overexpression can lead to increased ferroptosis in HCC cells, and CLTRN can enhance the radiosensitivity of HCC cells through the ferroptosis pathway. a Determination of iron content in cell lysates from different groups. b Measurement of ROS levels in different groups of cells. c Observation of mitochondrial changes in different groups of cells using transmission electron microscopy (red arrow indicates mitochondria in HCC cells), Scale bars: 2 μm. Mitochondria in the CLTRN overexpression group were significantly smaller, with increased membrane density and reduced mitochondrial ridges. d Changes in the expression of ferroptosis-related proteins in HCC cells upon CLTRN overexpression. PTGS2, NOX1, and ACSL4 were upregulated while GPX4, SLC7A11, and FTH1 were downregulated. The data are expressed in terms of mean ± SD (Student's t-test; ** P < 0.01; *** P < 0.001;****P < 0.0001).

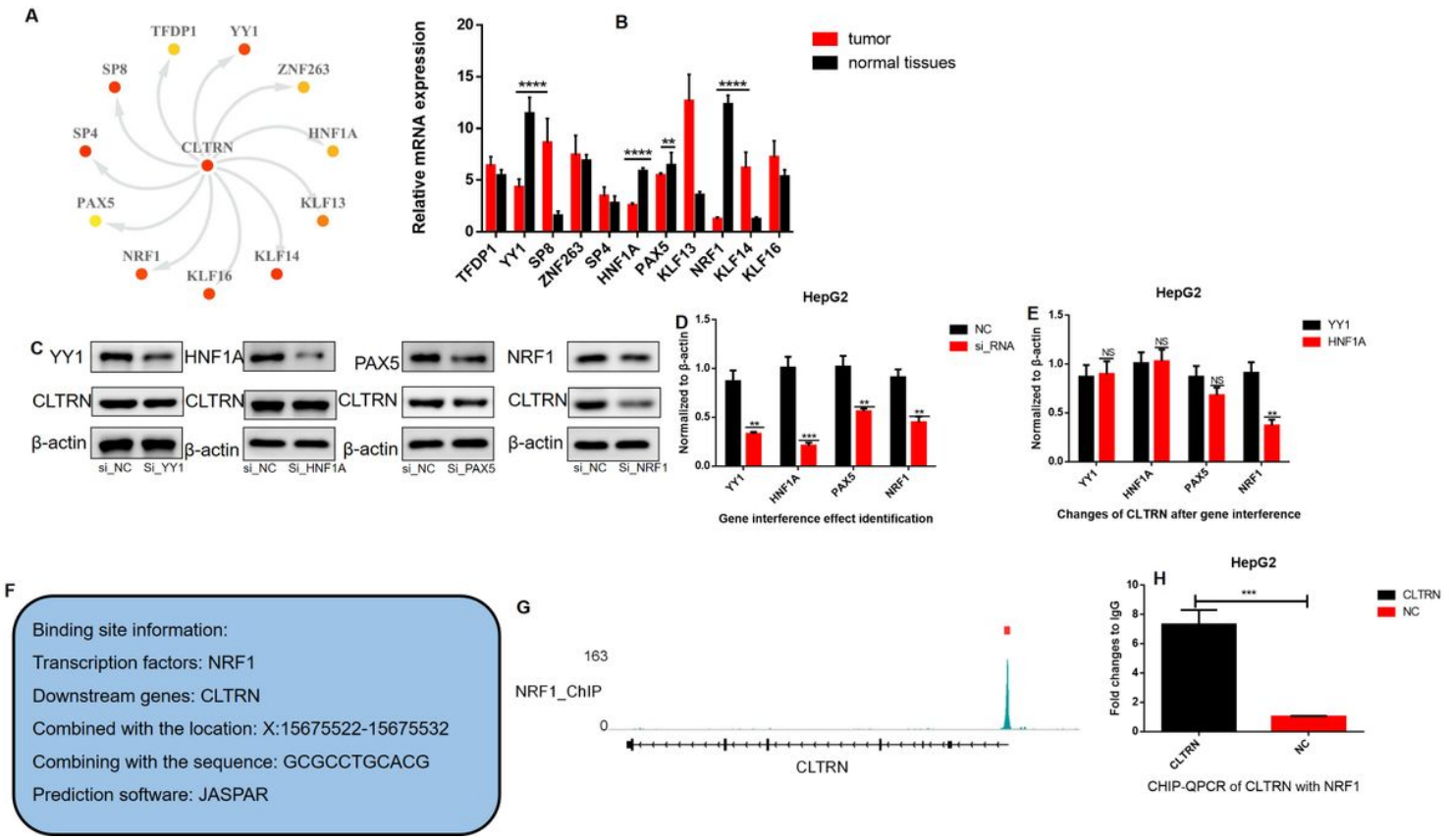

Figure 7

NRF1 is the upstream transcription factor of CLTRN in HCC cells. a The JASPAR website predicts possible upstream transcription factors of CLTRN with p < 0.01 as a premise. b Predictive gene expression in HCC and paracancer tissues; the expression of YY1, HNF1A, PAX5, and NRF1 was low in HCC tissues and high in paracancer tissues, similar to the pattern of CLTRN expression. c-e CLTRN expression in HepG2 cell lines after interference with YY1, HNF1A, PAX5, and NRF1. When NRF1 activity was impaired, CLTRN expression was significantly inhibited, which was different from that observed for the other three genes. f The JASPAR website predicts the binding sites of NRF1 and CLTRN. g Chip-seq data of NRF1 in the HepG2 cell line showed that NRF1 binds to CLTRN DNA. h NRF1 binding to CLTRN at the predicted sites was verified in HepG2 cells. The data are expressed in terms of mean ± SD (Student's t-test; ** P < 0.01; *** P < 0.001;****P < 0.0001; NS no significance).

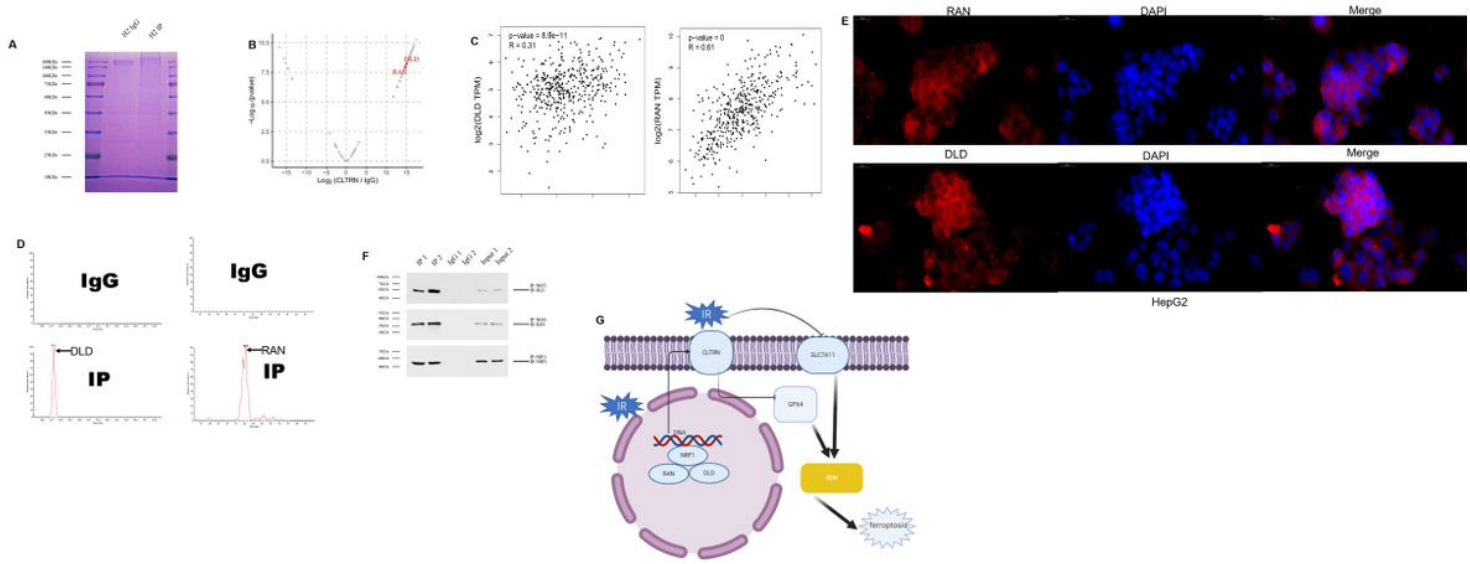

Figure 8

RAN and DLD are NRF1 interaction proteins in HCC cells. a Immunoprecipitation with the NRF1 antibody in HepG2 cells and staining with Coomassie blue. b The results of mass spectrometry are shown in volcanograms. c The proteins detected by mass spectrometry were screened using GEPIA and Uniprot databases. d RAN and DLD peptide profiles were analyzed using mass spectrometry. e Immunofluorescence analysis was performed to verify the localization of RAN and DLD in HepG2 cells; both were observed to be localized to the nucleus, Scale bars: 20 μm. f Co-immunoprecipitation experiment for verifying that RAN and DLD are interaction proteins of NRF1. g CLTRN, regulated by the NRF1/RAN/DLD protein complex, inhibits glutathione metabolism and increases ferroptosis, and thereby enhances the radiosensitivity of HCC cells.

Supplementary Files

This is a list of supplementary files associated with this preprint. Click to download.

- tables4.docx
- tables4.docx
- tables3.docx
- tables3.docx
- tables2.docx
- tables2.docx
- tables1.docx
- tables1.docx
- FigS1.jpg
- FigS1.jpg